IEEE Access
Multidisciplinary | Rapid Review | Open Access Journal

Received January 23, 2020, accepted January 30, 2020, date of publication February 6, 2020, date of current version February 14, 2020.

Digital Object Identifier 10.1109/ACCESS.2020.2972151

A New Feature-Based Wavelet Completed Local Ternary Pattern (Feat-WCLTP) for Texture Image Classification

ABEER MOH'D SHAMAILEH, TAHA H. RASSEM, (Senior Member, IEEE), LIEW SIAU CHUIN, AND OSAMA NAYEL AL SAYAYDEH

Faculty of Computing, College of Computing and Applied Sciences, University Malaysia Pahang, Kuantan 26300, Malaysia

Corresponding author: Taha H. Rassem (tahahussein@ump.edu.my)

This work was supported in part by the Ministry of Eduction under Grant FRGS/1/2018/ICT02/UMP/02/6 (RDU190173), and in part by the University Malaysia Pahang under Grant RDU180365 and Grant RDU190333.

ABSTRACT LBP is one of the simplest yet most powerful feature extraction descriptors. Many descriptors based on LBP have been proposed to improve its performance. Completed Local Ternary Pattern (CLTP) is one of the important LBP variants that was proposed to overcome LBP's drawbacks. However, despite the impressive performance of CLTP, it suffers from some limitations, such as high dimensionality, thereby leading to higher computation time and may affect the classification accuracy. In this paper, a new rotation invariant texture descriptor (Feat-WCLTP) is proposed. In the proposed Feat-WCLTP descriptor, first the redundant discrete wavelet transform RDWT is integrated with the original CLTP. Then, CLTP is extracted based on the LL wavelet coefficients. Next, the mean and variance features are used to describe the magnitude information instead of using P-dimensional features as the normal magnitude components of CLTP. Reducing the number of extracted features positively affected the computational complexity of the descriptor and the dimensionality of the resultant histogram. The proposed Feat-WCLTP is evaluated using four texture datasets and compared with some well-known descriptors. The experimental results show that Feat-WCLTP outperformed the other descriptors in terms of classification accuracy. It achieves 99.66% in OuTex, 96.89% in CUReT, 95.23% in UIUC and 99.92% in the Kylberg dataset. The experimental results showed that the Feat-WCLTP not only overcomes the CLTP's dimensionality problem but also further improves the classification accuracy.

INDEX TERMS Texture classification, local binary pattern (LBP), completed local ternary pattern (CLTP), RDWT.

I. INTRODUCTION

Texture classification is increasingly recognised as a serious issue in the texture analysis field [1]. As it plays a key role in a wide variety of real-life applications such as medical images analysis [2]–[4], human detector [5], human action recognition [6], manufacturing industry [7], image segmentation [8], remote sensing [9], object tracking [10], [11], face recognition [12], [13], and image retrieval [14], [15]. Generally, texture classification aims to design an algorithm that can address a sample image to reference image in a predefined image database based on image texture property. The extraction of efficient and robust texture feature is the main task of texture classification [16]–[18]. The main challenge of texture classification is how to deal with external changes in the imaging conditions such as rotation, scaling, illumination, viewpoint and noise. Accordingly, numerous numbers of descriptors have been developed and introduced over the past decades. The common purpose of all descriptors is how to extract powerful texture features that are robust to intra-class variance and can perform well in real-life applications.

Of the many descriptors, Local Binary Pattern (LBP) have brightened up as one of the most eminent and widely studied texture descriptor [19]. LBP was first proposed two decades ago by [20]. It was initially defined within the concept of 8 grey pixels with a centre pixel. The LBP encoding

The associate editor coordinating the review of this manuscript and approving it for publication was Wenming Cao.

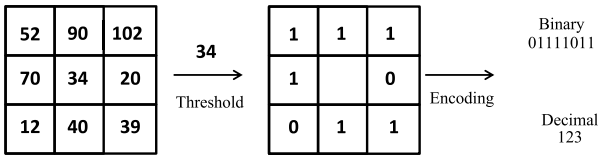

FIGURE 1. LBP encoding process.

process is illustrated in Figure 1, where the grey-level difference between the centre pixel and its neighbourhood pixel is calculated. The neighbourhood pixel is set to 1 if the difference is positive or 0 if it is negative; then, these values are used to obtain a binary code, which is generated later to represent a histogram that describes the image texture. LBP gained high popularity due to its superior advantages (i.e. simplicity, flexibility, distinguishing ability and the invariance against monotonic grey level changes), which make LBP a preferred choice for many texture analysis applications. However, LBP suffers from several major limitations such as noise sensitivity and different patterns may be sometimes classified falsely as shown in Figures 2 and 3. In addition that the reliability of LBP decreases remarkably under the variance in rotation and illumination.

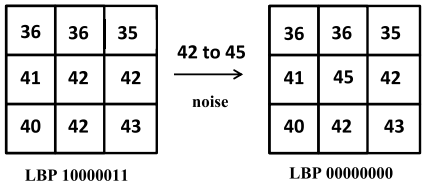

FIGURE 2. Example of the LBP operator's noise sensitivity.

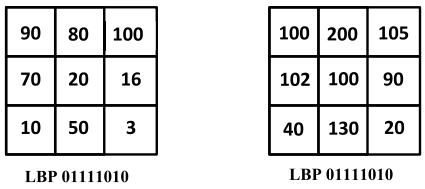

FIGURE 3. Example of classifying falsely problem.

Consequentially, a numerous number of LBP variants have been developed to overcome the aforementioned limitations as well as enhancing the classification performance of LBP such as Local Ternary Pattern (LTP), which is mainly designed to overcome the noise sensitivity problem [21]. The LTP local difference quantized into three levels, where the neighbour pixel values are encoded into 3 values instead of 2 values using a threshold value. But LTP is no longer invariant to grey-scale changes. With the same motivation, the Soft LBP (SLBP) was designed by [22]. SLBP generates multiple local binary patterns at every pixel position. Based on SLBP, the Noise Resistant Local Binary Pattern NRLBP is proposed where the small pixel difference encoded as an undetermined bit, then determine its value depending on the other bits of the LBP code [23]. Some other descriptors are designed to make better use of the nonuniform patterns instead of dismissing them and provide more noise resistance such as Novel Extended Local Binary Pattern (NELBP) [16] and Noise Tolerant Local Binary Pattern (NTLBP) [24]. However, these descriptors suffer from common serious drawback which is the limited neighbourhood size that leads to high computational complexity in case of generalization to larger scales [25]. On the other hand, many researchers have tended to focus on enhancing the discriminative power of LBP and improve the rotation invariant texture classification results by combined multiple types of local difference features such as Completed Local Binary Pattern (CLBP) [26] where the feature extraction including the information from the sign, magnitude and centre pixels. Then the information used to construct three operators, namely, CLBP_S, CLBP_M and CLBP_C. However, the CLBP suffers from some problems such as similar sizes of the dimensionality of the CLBP_M and the CLBP_S, which means that the size of the histogram grows sharply; and the need to exploit the complementary between the sign component and the magnitude component. Similar to CLBP, the Completed Local Binary Count(CLBC) was proposed by [27]. CLBC used different coding scheme where it depends on counting the number of values of 1's that resulted from the thresholding step without the encoding step. CLBC could achieve similar accurate classification rates as CLBP, as well as it reduces the computational complexity for the training and classification process. However, both of CLBP and CLBC are sensitive to noise. To overcome the noise sensitivity issue, Completed Local Ternary Pattern (CLTP) is proposed by predefining threshold value [28]. However, CLTP suffers from two main limitations which are the high dimensionality, where the size of CLTP is double that of CLBP, thereby increasing the computation time and needing a large memory space. Moreover, it may affect classification accuracy. In addition, the selecting of the threshold value in CLTP is manually based. On the basis of CLTP limitations, in this paper, we introduce a new texture descriptor namely, Feat-WCLTP, to enhance CLTP's performance and reduce its dimensionality. In the Feat-WCLTP descriptor, first, the redundant discrete wavelet transform RDWT is integrated with the original CLTP. Extracting CLTP in wavelet transform will help to increase the classification accuracy due to RDWT's shift-invariant property. RDWT decomposes the image into four sub-bands (LL, LH, HL, HH). Then, CLTP is extracted based on the LL wavelet coefficients. Next, the mean and variance features as explained in [29] are used to describe the magnitude information instead of using P-dimensional features as the normal magnitude components of CLTP. Using these two features help to reduce the dimensionality of CLTP as well as improve the performance since they provide better complementarity to the sign information. Finally, the centre information also included and used to build the centre operator. The three Feat-WCLTP operators are combined to represent the final histogram. The experimental results show that Feat-WCLTP can enhance CLTP performance and reduces the high dimensionality.

The rest of this paper is organized as follows. Section 2 reviews some previous descriptors such as LBP, LTP, CLBP, and CLTP. While section 3 presents the proposed Feat-WCLTP descriptor. Section 4 shows the experimental results and discussions. Finally, Section 5 concludes the paper.

II. RELATED WORK

In this section, a brief review of the different types of texture descriptors are given which are LBP, LTP, CLBP and CLTP.

A. LOCAL BINARY PATTEN (LBP)

The initial LBP method proposed by [20] was used to extract a texture feature. It provides the local measure of image contrast. LBP has initially been defined within the concept of 8 pixels and grey value centre pixel. The grey level variance between the centre pixel and its neighbourhood pixel is calculated. The neighbourhood pixels are set to 1 if the variance is positive or 0 if it's negative; as shown in Figure 1, then these values are used to obtain a binary code which is generated later to represent a histogram that describes the image texture. The LBP was developed based on the use of differently-sized neighbourhoods with the aid of asymmetric circle neighborhood defined by R and P [19]. Mathematically, LBP is defined as:

$$LBP_{P,R} = \sum_{p=0}^{P-1} 2^p s(i_p - i_c), \quad s(x) = \begin{cases} 1, & x \geq 0 \\ 0, & x < 0 \end{cases} \tag{1}$$

where i_c and i_p point out to the grey values of the centre pixel and the neighbor pixel, R represents the radius of the circle, and P is the number of neighborhood pixels. The neighbors' pixels that do not fall exactly in the center of pixels are estimated by interpolation. Together with this generalization, authors presented ''uniform patterns'' of LBP [19]. LBP is called uniform if its uniformity measure is equal to at most 2. Uniformity (U) is the number of bitwise transitions from 0 to 1 or 1 to 0 when the bit pattern is considered circular. In uniform pattern LBP, each pattern will be assigned by a separate label, and all non-uniform patterns will be assigned to single label. This makes the uniform pattern LBP ($LBP^{u2}_{(P,R)}$) histogram size smaller compared to the original LBP. For P neighbours, there will be $P*(P-1)+3$ different texture features as opposed to 2^P features in the original LBP. To achieve rotation invariance, a locally rotation invariant pattern is presented in [19] as:

$$LBP^{riu2}_{P,R} = \begin{cases} \sum_{p=0}^{P-1} s(i_p - i_c) & if\ U(LBP_{P,R}) \leq 2 \\ P+1 & otherwise \end{cases} \tag{2}$$

where

$$U(LBP_{P,R}) = |s(i_{P-1} - i_c) - s(i_0 - i_c)| + \sum_{p=1}^{P-1} |s(i_p - i_c) - s(i_{p-1} - i_c)| \tag{3}$$

B. LOCAL TENARY PATTERN (LTP)

In [21], the authors modified the general LBP model with a view to overcome the sensitivity-to-noise issue by adding a threshold value (t) and encoding the neighbor pixel values into 3-values instead of 2-values. Mathematically LTP can be presented as follows:

$$LTP_{P,R} = \sum_{p=0}^{P-1} 2^p s(i_p - i_c), \quad s(x) = \begin{cases} 1, & x \geq t, \\ 0, & -t < x < t, \\ -1, & x < -t, \end{cases} \tag{4}$$

where i_c, i_p, R and P are defined before in Equation 1 and t denotes the user threshold. According to Equation 4, two parts are the output of the encoding process. The upper and lower patterns' histograms are concatenated together as the final representation of LTP.

C. COMPLETED LOCAL BINARY PATTERN (CLBP)

CLBP was introduced by [26] as a new texture descriptor. In CLBP, the authors adopted a broader perspective for feature extraction more than LBP by including the information from the magnitude vectors and the centre pixels. The local difference is disassembled into two complementary components which are the the sign component $s_p = s(i_p - i_c)$ and magnitude component $m_p = |i_p - i_c|$. The sign component is used to build *CLBP_S* operator, which is equivalent to the conventional LBP. The magnitude component is used to construct the *CLBP_M* operator that measures the local variance of the magnitude. *CLBP_S* and *CLBP_M* can be expressed as follows:

$$CLBP\_S_{P,R} = \sum_{p=0}^{P-1} 2^p s(i_p - i_c), \quad s_p = \begin{cases} 1, & i_p \geq i_c, \\ 0, & i_p < i_c, \end{cases} \tag{5}$$

$$CLBP\_M_{P,R} = \sum_{p=0}^{P-1} 2^p t(m_p, c),$$

$$t(m_p, c) = \begin{cases} 1, & |i_p - i_c| \geq c, \\ 0, & |i_p - i_c| < c, \end{cases} \tag{6}$$

where i_c, i_p, R and P are defined before in Equation 1, m_p is the magnitude component and c denotes the mean value of m_p.

The *CLBP_C* operator is constructed by thresholding the centre pixel of the 3×3 neighbourhood pattern at the average greyscale value of the whole image. It is mathematically expressed as follows:

$$CLBP\_C_{P,R} = t(i_c, c_I) \tag{7}$$

where i_c denotes the grey value of the centre pixel of the pattern, and c_I denotes the average grey level of the entire image. The three operators could be combined into joint or hybrid distributions [26].

D. COMPLETED LOCAL TERNARY PATTERN (CLTP)

In [28], the authors introduced the CLTP descriptor by combining CLBP and LTP. In CLTP, the local difference is

decomposed into four complementary components; the first two are the upper and lower sign components, and the second two are the upper and lower magnitude components, which can be expressed as follows:

$$s_p^{upper} = s(i_p - (i_c + t)), \quad s_p^{lower} = s(i_p - (i_c - t)) \tag{8}$$

$$m_p^{upper} = |i_p - (i_c + t)|, \quad m_p^{lower} = |i_p - (i_c - t)| \tag{9}$$

Then the sign components are used to build the $CLTP\_S_{P,R}^{upper}$ and $CLTP\_S_{P,R}^{lower}$ as follows:

$$CLTP\_S_{P,R}^{upper} = \sum_{p=0}^{P-1} 2^p s(i_p - (i_c + t)),$$

$$s_p^{upper} = \begin{cases} 1, & i_p \geq i_c + t, \\ 0, & otherwise, \end{cases} \tag{10}$$

$$CLTP\_S_{P,R}^{lower} = \sum_{p=0}^{P-1} 2^p s(i_p - (i_c - t)),$$

$$s_p^{lower} = \begin{cases} 1, & i_p < i_c - t, \\ 0, & otherwise, \end{cases} \tag{11}$$

where $\imath_c$, i_p, R and P are defined in Equation 1, and t is the threshold value.

The $CLTP\_S_{P,R}^{upper}$ and $CLTP\_S_{P,R}^{lower}$ operators are then concatenated to form $CLTP\_S_{P,R}$ as follows:

$$CLTP\_S_{P,R} = [CLTP\_S_{P,R}^{upper} \quad CLTP\_S_{P,R}^{lower}] \tag{12}$$

With the use of m_p^{upper} and m_p^{lower}, the $CLTP\_M_{P,R}$ is built as follows

$$CLTP\_M_{P,R}^{upper} = \sum_{p=0}^{P-1} 2^p t(m_p^{upper}, c),$$

$$t(m_p^{upper}, c) = \begin{cases} 1, & |i_p - (i_c + t)| \geq c, \\ 0, & |i_p - (i_c + t)| < c, \end{cases} \tag{13}$$

$$CLTP\_M_{P,R}^{lower} = \sum_{p=0}^{P-1} 2^p t(m_p^{lower}, c),$$

$$t(m_p^{lower}, c) = \begin{cases} 1, & |i_p - (i_c - t)| \geq c, \\ 0, & |i_p - (i_c - t)| < c, \end{cases} \tag{14}$$

where i_c, i_p, R and P are defined previously in Equation 1 and c is the mean value of the magnitude component.

$$CLTP\_M_{P,R} = [CLTP\_M_{P,R}^{upper} \quad CLTP\_M_{P,R}^{lower}] \tag{15}$$

Then, $CLTP\_C_{P,R}^{upper}$ and $CLTP\_C_{P,R}^{lower}$ can be mathematically expressed as follows:

$$CLTP\_C_{P,R}^{upper} = t(i_c^{upper}, c_I) \tag{16}$$

$$CLTP\_C_{P,R}^{lower} = t(i_c^{lower}, c_I) \tag{17}$$

where $i_c^{upper} = i_c + t$, $i_c^{lower} = i_c - t$ and c_I is the average pixel intensities of the whole image.

The final CLTP is built the same as the CLBP by combining the three CLTP operators into joint or hybrid distributions to build the final histogram. Although the above texture classification descriptors can achieve good performances, they are not adequate in classifying rotational and noisy textures. Therefore, we propose a new texture classification descriptor named Feat-WCLTP, which can achieve better classification performances as well as reduce the computational time.

III. PROPOSED FEAT-WCLTP

In this section, we introduce the proposed Feat-WCLTP descriptor. The proposing Feat-WCLTP consists of two key stages, i.e. integrating RDWT with CLTP and introducing WCLTP to enhance the classification performance and proposing a new feature-based texture descriptor. Figure 4 presents the general framework of our proposed texture classification method.

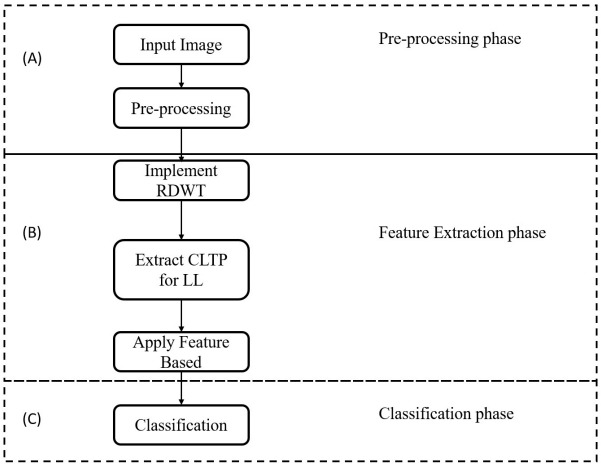

FIGURE 4. General framework of our proposed texture classification method (Feat-WCLTP).

A. INTEGRATING RDWT WITH CLTP (WCLTP)

In image processing, the method of transforming the images from the spatial forms (pixel values) to the wavelet form has been used to enhance many applications due to the properties of WTs, such as the ability to analyse data at different scales and the low computational complexity [30].

RDWT transform is considered one of the robust WTs. It was proposed to overcome the limitations of DWT [31]. The downsampling in DWT gains shift variance even for a slight shift in the input image, thereby leading to incorrect feature extraction. RDWT addresses the shift variance problem of DWT. It decomposes an image into four sub-bands, where the size of each sub-band equals the size of the original image, unlike DWT where the sub-band size is only the half size of the original image. As a result, the important textures in the image will be at the same spatial location in each sub-band, thereby ensuring accurate capture of the local texture and its exact measure. The implementation steps of the proposed WCLTP are described as follows: Firstly, RDWT is applied to the preprocessed input image and decomposes the image into four sub-bands: *LL*, *HL*, *LH* and *HH*. *LH*, *HL* and *HH* represent the horizontal, vertical and diagonal

detail, respectively. *LL* is approximate for the input image; thus, the power is more compact in the *LL* sub-band where contains the signifcant infomration of the image and has less noise component. Therefore, the *LL* sub-band is selected.

Then, *CLTP_S*, *CLTP_M* and *CLTP_C* are extracted from the *LL* sub-band. *WCLTP_S*, *WCLTP_M* and *WCLTP_C* are combined in different ways to evaluate the effectiveness of the WT. Figure 5 shows the WCLTP extraction process.

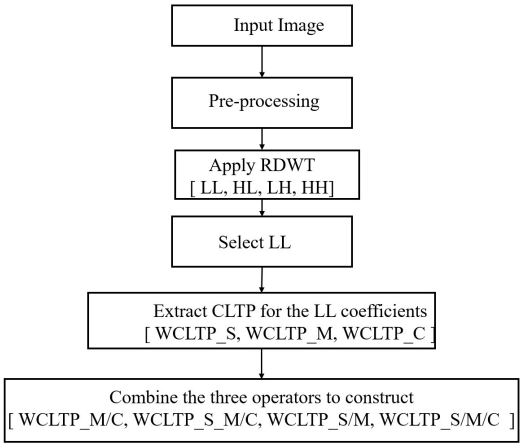

FIGURE 5. Flowchart of WCLTP extraction process.

WCLTP_S, *WCLTP_M* and *WCLTP_C* operators are combined into joint or hybrid distributions to build the final operator histogram similar to CLTP. The operators of the same type of pattern, i.e., the upper and the lower pattern, are combined firstly into joint or hybrid distributions. In this paper, we firstly evaluate the WCLTP independently to show the effectiveness of using wavelet in improving the CLTP's performance.

B. FEATURE-BASED WCLTP

The WCLTP mentioned in the previous stage enhances the classification performance of CLTP. However, it inherits the high dimensionality drawback of traditional CLTP. Where the size of the resulting histogram is too large. The high dimensionality negatively affected the performance of the descriptor and increased the running time. Moreover, high dimensionality needs large storage space. Therefore, we try to overcome the high dimensionality problem as well as maintain the improved performance through the following steps:

1) The sign component Feat-WCLTP_S
The Feat-WCLTP_S is equal to WCLTP_S in order to retain the powerful features of the sign component. It can be expressed mathematically as follows: Firstly, the upper and lower sign components of local difference are calculated as in Equation 8.
Then the sign components are used to build the $Feat - WCLTP\_S^{upper}_{P,R}$ and $Feat - WCLTP\_S^{lower}_{P,R}$, as follows:

$$Feat - WCLTP\_S^{upper}_{P,R} = \sum_{p=0}^{P-1} 2^p s(i_p - (i_c + t)),$$
$$s_p^{upper} = \begin{cases} 1, & i_p \geq i_c + t, \\ 0, & otherwise, \end{cases} \quad (18)$$
$$Feat - WCLTP\_S^{lower}_{P,R} = \sum_{p=0}^{P-1} 2^p s(i_p - (i_c - t)),$$
$$s_p^{lower} = \begin{cases} 1, & i_p < i_c - t, \\ 0, & otherwise, \end{cases} \quad (19)$$

where $\imath_c$, i_p, R and P are defined in Equation 1, and t is the threshold value.
The $Feat - WCLTP\_S^{upper}_{P,R}$ and $Feat - WCLTP\_S^{lower}_{P,R}$ operators are then concatenated to form $Feat - WCLTP\_S_{P,R}$ as follows:

$$Feat - WCLTP\_S_{P,R} = [Feat - WCLTP\_S^{upper}_{P,R} \; Feat - WCLTP\_S^{lower}_{P,R}] \quad (20)$$

Figure 6 illustrates an example of the $Feat - WCLTP\_S_{P,R}$ calculation process.

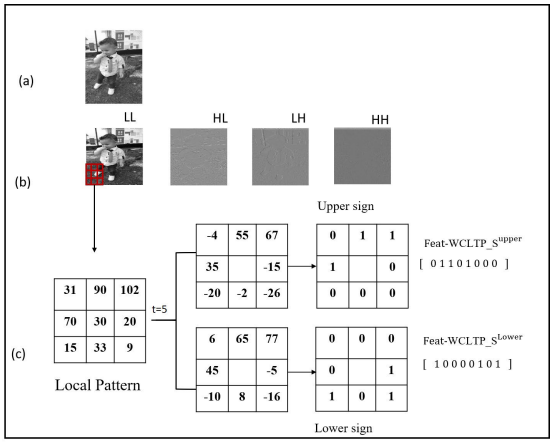

FIGURE 6. Example of Feat-WCLTP sign extraction process.

2) The magnitude component Feat-WCLTP_M
In [26], the authors in their major study confirmed by analysis that the sign vector of local difference possesses more information than the magnitude vector. This situation explains why texture classification using the sign operator achieves much higher accuracy than that achieved by the magnitude operator. On the basis of this finding, we try to overcome the high dimensionality problem by modifying the structure of the magnitude operator and reducing the number of extracted features. In this case, we propose to reduce the number of features generated from the magnitude from P-dimensional features to only two-dimensional features, which are the mean and variance of the magnitude vector. The mean feature μ indicates the average

difference between the centre pixel and its neighbours, while the variance σ^2 indicates the total changes in the magnitude vector m_p.

Mathematically, to compute $Feat - WCLTP_M$, the upper and lower magnitude components are calculated as Equation 9. The mean and the variance of the magnitude vector m_p can be calculated using the following equations:

$$\mu^{upper} = \frac{1}{P}\sum_{p=0}^{P-1} m_p^{upper} \tag{21}$$

$$\mu^{lower} = \frac{1}{P}\sum_{p=0}^{P-1} m_p^{lower} \tag{22}$$

$$\sigma^{upper} = \frac{1}{P}\sum_{p=0}^{P-1} (m_p^{upper} - \mu^{upper})^2 \tag{23}$$

$$\sigma^{lower} = \frac{1}{P}\sum_{p=0}^{P-1} (m_p^{lower} - \mu^{lower})^2 \tag{24}$$

where P is the number of neighbouring pixels.

The mean and variance are the average values of all P elements in the magnitude vector. Thus, using these features can diminish the impact of noise, rotation and illumination. Moreover, when using these two features, all non-uniform patterns do not need to be integrated into a single bin as in CLBP_M and CLTP_M, which means better complementary information will be provided to the sign component. This approach will positively reflect on the descriptor performance. However, the mean and variance values are needed to encode because they are continuous values, which means they cannot be used directly in the classification process. Thus, to convert them to discrete values, an adaptive threshold method is used. In this method, the input image is divided into four equal non overlapping sub-images. Then, a threshold value for each mean and variance in each sub-image is calculated as follows:

$$T_\mu^{upper} = \frac{1}{N}\sum_{n=0}^{N-1} \mu^{upper} \tag{25}$$

$$T_\mu^{lower} = \frac{1}{N}\sum_{n=0}^{N-1} \mu^{lower} \tag{26}$$

where N is the number of local patterns in each sub-image. The following equations are used to determine the threshold values for upper and lower variances.

$$T_\sigma^{upper} = \frac{1}{N}\sum_{n=0}^{N-1} \sigma^{upper} \tag{27}$$

$$T_\sigma^{lower} = \frac{1}{N}\sum_{n=0}^{N-1} \sigma^{lower} \tag{28}$$

Using this threshold method helps properly exploit the relationships between pixels. The upper and lower mean and variance features are converted to binary format by using the following equations:

$$F_\mu^{upper}(i_c) = s(\mu^{upper} - T_\mu^{upper}) \tag{29}$$

$$F_\mu^{lower}(i_c) = s(\mu^{lower} - T_\mu^{lower}) \tag{30}$$

$$F_\sigma^{upper}(i_c) = s(\sigma^{upper} - T_\sigma^{upper}) \tag{31}$$

$$F_\sigma^{lower}(i_c) = s(\sigma^{lower} - T_\sigma^{lower}) \tag{32}$$

where i_c is the centre pixel. In the Equations 29 to 32, s(x) is the same as defined in Equation 1.

The upper and lower features used to build the final $Feat - WCLTP_M$ as follows:

$$Feat - WCLTP\_M_{P,R}^{upper} = [F_\mu^{upper} \quad F_\sigma^{upper}] \tag{33}$$

$$Feat - WCLTP\_M_{P,R}^{lower} = [F_\mu^{lower} \quad F_\sigma^{lower}] \tag{34}$$

$$Feat - WCLTP\_M_{P,R} = [Feat - WCLTP\_M_{P,R}^{upper} \; Feat - WCLTP\_M_{P,R}^{lower}] \tag{35}$$

This process can be explained using an example as shown in Figure 7.

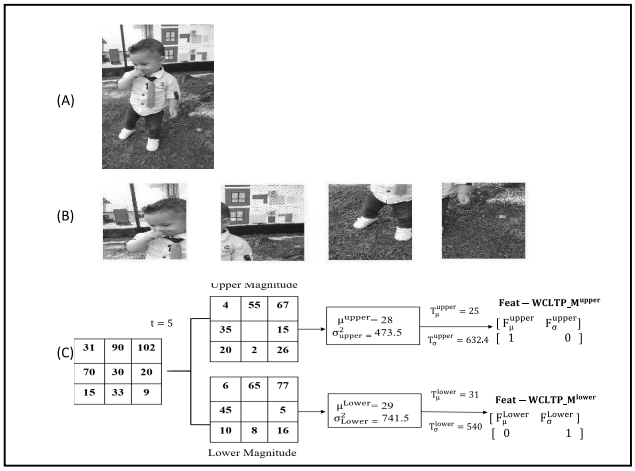

FIGURE 7. Example of the calculation process for magnitude component for Feat-WCLTP.

Using the mean and variance features makes the dimensionality of the magnitude become rather small as $((2\times2)\times2)$. To extract more discriminative information from the centre pixel, it is encoded in the same way as the mean and variance. The threshold value for the centre pixel is the average grey values of the current sub-image

$$T_c^{upper} = \frac{\sum_{n=0}^{N-1} i_c^{upper}}{N} \tag{36}$$

$$T_c^{lower} = \frac{\sum_{n=0}^{N-1} i_c^{lower}}{N} \tag{37}$$

where i_c^{upper} and i_c^{lower} are the centre pixels with adding and subtracting the threshold value, respectively.

To construct the centre operator $Feat - WCLTP\_C$, the following equations are used:

$$F_c^{upper}(i_c) = s(i_c^{upper} - T_c^{upper}) \quad (38)$$

$$F_c^{lower}(i_c) = s(i_c^{lower} - T_c^{lower}) \quad (39)$$

where i_c is the centre pixel.

$$Feat - WCLTP\_C = [F_c^{upper}(i_c) \quad F_c^{lower}(i_c)] \quad (40)$$

3) Combining three components Feat-WCLTP
After computing all features from $Feat - WCLTP\_C$, $Feat - WCLTP\_M$ and $Feat - WCLTP\_S$, the three operators are integrated into joint or hybrid distributions to build the final histogram as *WCLTP*. The $Feat - WCLTP$ makes the dimensionality of the final histogram become rather small as $((P+2) \times (2 \times 2) \times 2) \times 2$. Table 1 shows the comparison results of the final histogram dimensionality of different descriptor.
From Table 1, we can notice that $LBP_{P,R}^{riu2}$ and *LTP* has the smallest histogram size, but they achieved much poor classification performance since they depend only on the sign operator. Despite that BRINT has low histogram dimensions relatively, its performance is poor comparing with another texture descriptors [3], [32], [33]

TABLE 1. Histogram size of various descriptors.

Descriptor	Histogram size for a single scale
LBP	2^P
LBP	$P \times R + 2$
LTP	$(P \times R + 2) \times 2$
CLBP	$(P \times R + 2) \times (P \times R + 2) \times 2$
CLBC	$(P \times R + 1) \times (P \times R + 1) \times 2$
BRINT	144
NRLBP	3^p
CLTP	$((P \times R + 2) \times (P \times R + 2) \times 2) \times 2$
WCLTP	$((P \times R + 2) \times (P \times R + 2) \times 2) \times 2$
Feat-WCLTP	$((P \times R + 2) \times (2 \times 2) \times 2) \times 2$

IV. EXPERIMENTAL RESULTS

To evaluate the effectiveness of the proposed work, we carried out a series of experiments on four representative texture datasets: CUReT [34], OuTex [35], UIUC [36] and Kylberg dataset [37]. Table 2 summarises the main characteristics of the datasets. The proposed descriptors are compared with some state-of-art LBP-based descriptors, which are the LBP [19], LTP [21], CLBP [26], CLBC [27] and CLTP [28]. In all experiements, the threshold value (t) is set to 5.

A. DISSIMILARITY MEASUREMENT

To measure the dissimilarity between two histograms, the chi-square statistic is used whereas the nearest neighbourhood classifier is used in classification. The following equation calculates the distance χ^2 between two histogram $H = hi$ and $K = ki$ where $(i = 1, 2, 3, 4, \cdots, B)$:

$$Dissimilarity_{\chi^2}(H, K) = \sum_{(i=1)}^{B} \frac{(h_i - k_i)^2}{(h_i + k_i)} \quad (41)$$

TABLE 2. The benchmark datasets used in the experiments.

Texture datasets	Classes	Sample per class	Total samples
OuTex TC-10	24	20	4320
OuTex TC-12	24	20	8640
CUReT	61	46	5612
UIUC	25	40	1000
Kylberg	28	160	4480

B. EXPERIMENTAL RESULTS ON THE OUTEX DATASET

For experiments on the, two suites (TC10) and (TC12), which are considered the two most well-known test suites in OuTex, were selected. Each of (TC10) and (TC12) has 24 texture classes captured under nine different rotation angles (0°, 5°, 10°, 15°, 30°, 45°, 60°, 75°, and 90°) and three uneven type of illumination source (“horizon”, “inca” and “t184”). Twenty 128×128 non-overlapping images are available for each rotation angle under a given illumination condition. For TC10, 480 images with “inca” illumination condition and 0° angle rotation were used as training set whereas the remaining 3840 images are used as the testing set. For TC12 the training set is the same as that of TC10 while 4320 images under “t184” or “horizon” illumination conditions were used as the testing set. Some images from the OuTeX dataset are shown in Figure 8. The experimental results of OuTex dataset are presented in Table 3.

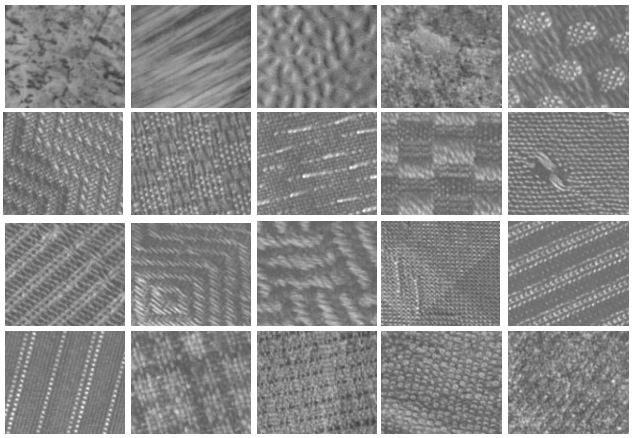

FIGURE 8. Some images from OuTeX dataset.

As shown in Table 3, the classification accuracy for the individual operator that depends on sign difference calculation is mostly greater than the accuracy achieved by

TABLE 3. Classification rates (%) on the OuTex dataset.

Method	R =1 , P = 8				R =2 , P = 16				R =3 , P = 24			
		TC12				TC12				TC12		
	TC10	T	H	Avg.	TC10	T	H	Avg.	TC10	T	H	Avg.
LBP	84.81	65.46	63.68	71.32	89.4	82.27	75.21	82.29	95.08	85.05	80.79	86.97
LTP	94.14	75.88	73.96	81.33	96.95	90.16	86.94	91.35	98.2	93.59	89.42	93.74
CLBP_S	84.41	65.46	63.68	71.18	89.4	82.26	75.2	82.29	95.07	85.04	80.78	86.96
CLBC_S	82.94	65.02	63.17	70.38	88.67	82.57	77.41	82.88	91.35	83.82	82.75	85.97
CLTP_S	94.14	75.88	73.96	81.33	96.95	90.16	86.94	91.35	98.2	93.59	89.42	93.74
WCLTP_S	92.97	83.56	80	85.51	94.97	92.04	86.81	91.27	97.89	93.87	90.51	94.09
CLBP_M	81.74	59.3	62.77	67.94	93.67	73.79	72.4	79.95	95.52	81.18	78.65	85.12
CLBC_M	78.96	53.63	58.01	63.53	92.45	70.35	72.64	78.48	91.85	75.59	74.58	80.67
CLTP_M	94.04	75.86	74.05	81.32	97.32	83.4	84.4	88.37	98	85.39	84.65	89.35
WCLTP_M	94.51	77.36	77.71	83.19	97.11	82.71	86.53	88.78	97.89	83.54	84.42	88.62
CLBP_M/C	90.36	72.38	76.66	79.8	97.44	86.94	90.97	91.78	98.02	90.74	90.69	93.15
CLTP_M/C	95.94	84.7	86.02	88.89	97.94	90.14	92.38	93.49	98.52	91.23	89.98	93.24
WCLTP_M/C	95.86	85.56	87.59	89.67	97.99	91.46	93.43	94.29	98.44	92.29	93.08	94.6
CLBP_S_M/C	94.53	81.88	82.52	86.31	98.02	90.99	91.08	93.36	98.33	94.05	92.4	94.93
CLTP_ S_M/C	96.43	84	86.85	89.09	98.44	92.14	92.8	94.55	98.98	95	92.94	95.64
WCLTP_ S_M/C	97.27	88.98	89.26	91.84	97.94	93.63	92.94	94.84	98.78	95.56	94.4	96.24
CLBP_S/M	94.66	82.75	83.14	86.85	97.89	90.55	91.11	93.18	99.32	93.58	93.35	95.42
CLBC_ S/M	95.23	82.13	83.59	86.98	98.1	89.95	90.42	92.82	98.7	91.41	90.25	93.45
CLTP_ S/M	96.41	82.85	84.81	88.02	97.84	92.06	92.69	94.2	99.04	94.14	95.59	96.26
WCLTP_ S/M	96.54	86.97	86.62	90.04	98.44	93.68	93.01	95.04	99.35	94.75	94.14	96.08
CLBP_S/M/C	96.56	90.3	92.29	93.05	98.72	93.54	93.91	95.39	98.93	95.32	94.53	96.26
CLBC_ S/M/C	97.16	89.79	92.92	93.29	98.54	93.26	94.07	95.29	98.78	94	93.24	95.34
CLTP_ S/M/C	96.88	90.25	92.92	93.35	98.83	93.59	94.26	95.56	99.17	95.67	94.28	96.37
WCLTP_ S/M/C	98.13	91.25	93.32	94.23	98.8	**95.6**	95.19	96.53	99.22	96.76	95.77	97.25
Feat-WCLTP_S/M/C	**99.04**	**92.57**	**94.07**	**95.23**	**99.3**	**95.6**	**95.18**	**96.69**	**99.66**	**98.06**	**98.83**	**98.85**

Bold values indicate the best result
* The results of LBP and LTP from [21]
** The results of CLBP, CLBC and CLTP from [29]

magnitude operators, thereby implying that the sign features are more discriminated than magnitude features. The *WCLTP* and *Feat* − *WCLTP* apparently outperformed the other descriptors in all experiments using OuTex (TC10) and (TC12). In the TC10 dataset, the *Feat* − *WCLTP* proved superior performance where the results were 99.04%, 99.30% and 99.66% at (P = 8, R = 1), (P = 16, R = 2) and (P = 24, R = 3), respectively. under the three radius values (R = 1, 2 and 3) followed by *WCLTP* which achieved 99.35% with $WCLTP\_S/M_{24,3}$, and the third rank for $CLBP\_S/M_{24,3}$ which had a 99.32% accuracy rate, while the worst result was obtained by $CLBP\_M_{8,1}$ with an accuracy of 81.74%. In TC12, although the WCLTP achieved better accuracy rate than others with an accuracy of 96.76% and 95.77% with both TC12(t) and TC12(h), respectively. However, the results of Feat-WCLTP were higher than those of WCLTP at an increased rate above 3%. Where it achieved 98.06% and 98.83% with both TC12(t) and TC12(h), respectively. Given that the OuTex dataset is subjected to illumination changes, the improved results confirmed that the proposed *Feat* − *WCLTP* is more robust to illumination variations.

C. EXPERIMENTAL RESULTS ON THE CURET DATASET

The CUReT dataset has 61 texture classes. Each class includes 205 texture images which are subjected to different illumination and viewpoint conditions. 118 images out of 250 images have viewing angles less than 60°. 92 images are selected after being converted to greyscale and cropped to 200×200 pixels. Out of 92 images, N images are selected and used as training data, while the remaining $(92-N)$ are used as testing data. The final classification accuracy is the average percentage over a hundred random splits. Some images from the CuReT dataset are shown in Figure 9. Table 4 shows the classification results for N = (6, 12, 23, 46) on CUReT dataset.

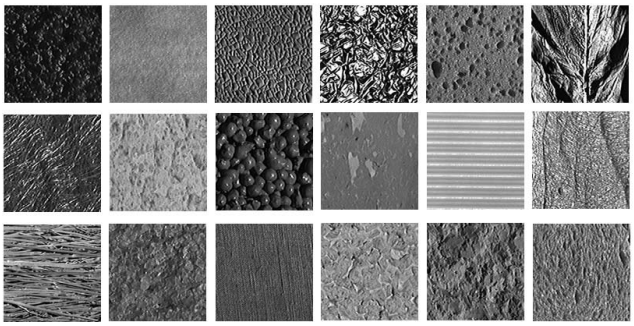

FIGURE 9. Some images from CuReT dataset.

Table 4 shows that the proposed *Feat* − *WCLTP* performs better than other descriptors on average. *Feat* − *WCLTP* achieved the highest classification accuracy rates of 96.12%, 96.42% and 96.89% at (P = 8, R = 1), (P = 16, R = 2) and (P = 24, R = 3), respectively. While the WCLTP classification accuracy reaches 96.57% with $WCLTP\_S/M/C_{24,3}$ and $CLTP\_S/M/C_{24,3}$ has an accuracy of 96.11%. However, *CLTP* and *CLBP* showed better performance in some cases in this dataset. The performance varies based on the texture pattern (i.e. R = 1, P = 8, R = 2, P = 16 and R = 3, P = 24) with a different number of training images. In general, the evaluation results confirmed that the WCLTP is more rotation invariant than other descriptors because of the RDWT's shift-invariance.

TABLE 4. Classification rates (%) on the CUReT dataset.

Descriptor	Parameters (R,P) . R =the radius of the circle, P =the number of neighbourhood pixels											
	P=8, R=1				P=16, R=2				P=24, R=3			
	6	12	23	46	6	12	23	46	6	12	23	46
LBP^{riu2}	60.36	69.05	74.64	81.32	63.38	72.7	79.28	84.53	67.86	75.51	81.65	86.35
LTP	65.17	74.61	80.85	87.74	68.72	80.18	86.17	91.16	72.76	82.42	87.19	91.52
CLBP_S	59	67.81	74.62	80.7	63.49	72.68	79.49	85.35	66.94	75.26	81.8	87.31
CLBC_S	56.88	66.21	72.89	78.82	60.42	68.95	74.42	79.78	60.82	70.57	74.21	80.14
CLTP_S	64.38	72.66	81.73	88.24	68.39	79.09	86.61	91.55	72.57	81.55	87.72	91.75
WCLTP_S	62.73	72.18	79.48	85.9	68.54	78.47	83.17	89.16	70.5	78.68	85.2	90.57
CLBP_M	51.77	60.33	67.73	75.16	58.557	68.28	76.11	83.03	62.57	71.93	79.89	68.49
CLBC_M	50.12	58.62	57.82	66.61	50.63	58.7	66.05	73.89	51.23	60.53	68.36	77.41
CLTP_M	61.37	71.17	80.53	86.67	63.33	74.47	82.14	88.83	67.14	76.93	85.16	90.52
WCLTP_M	58.22	67.94	76.14	83.74	64.49	72.82	82.19	88	64.89	74.86	82.89	89.11
CLBP_M/C	56.53	67.15	75.58	82.97	64.81	75.56	82.98	89.75	68.71	78.54	86.04	91.65
CLTP_M/C	62.07	72.94	82.26	88.98	66.77	77.12	85.51	91.67	70.1	80.12	89.02	93.58
WCLTP_M/C	61.83	73.01	81.68	88.96	66.61	77.96	86.43	92.52	71.55	80.99	88.2	93.6
CLBP_S_M/C	66.63	76.54	85.02	90.55	70.27	80.47	87.57	92.78	73.29	82.28	89.28	94.07
CLTP_S_M/C	67.54	78.89	85.46	91.27	71.55	82.16	87.82	94.04	74.36	85.14	91.03	94.69
WCLTP_S_M/C	67.7	77.89	86.81	92.63	70.12	83.44	88.94	94.06	74.55	83.37	90.34	94.87
CLBP_S/M	71.86	82.27	88.57	93.46	74.63	83.44	89.67	93.85	74.95	84.3	90.83	94.53
CLBC_S/M	69.89	79.88	86.62	93.1	72.16	81.71	89.6	93.78	70.52	81.57	89.12	93.6
CLTP_S/M	71.3	82.37	89.2	93.5	74.14	84.42	90.78	95.06	76.49	85.11	92.02	95.63
WCLTP_S/M	70.63	81.67	88.46	93.69	75.79	84.87	90.87	95.49	76.31	85.25	91.59	95.43
CLBP_S/M/C	74.35	**85.06**	**91.52**	95.07	76.07	85.73	92.15	95.67	76.8	86.54	92	95.72
CLBC_S/M/C	72.85	82.92	90.12	94.78	75.17	85.91	91.3	95.39	73.18	84.07	90.55	95.26
CLTP_S/M/C	**75.18**	84.06	90.45	94.78	77.72	85.54	92.44	95.95	77.97	**87.5**	92.72	96.11
WCLTP_S/M/C	72.81	83.96	91.1	95.86	77.85	**86.68**	92.53	96.27	78.3	87.27	**93.28**	96.57
Feat-WCLTP_S/M/C	73.53	84.86	91.48	**96.12**	**78.41**	86.15	**92.71**	**96.42**	**78.49**	87.13	92.87	**96.89**

Bold values indicate the best result
* The results of LBP and LTP from [21]
* The results of CLBP, CLBC and CLTP from [29]

D. EXPERIMENTAL RESULTS ON THE UIUC DATASET

The UIUC dataset includes 25 texture classes. Each class has 40 images captured in different illumination conditions and viewing points. Figure 10 shows some sample images in the UIUC dataset. Following the same procedure in [28], different training images (N) are randomly selected for each class where (N = 5, 10, 15, 20). The remaining (40-N) images are used as the test set. Each random selection is repeated 100 times to obtain statistically valid experimental results. The experimental results of the UIUC dataset are shown in Table 5.

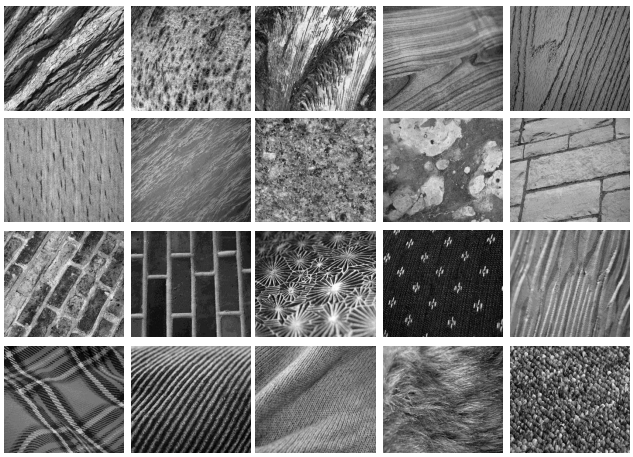

FIGURE 10. some sample images in UIUC dataset.

A significant observation that can be drawn from Table 5 is that the UIUC dataset is difficult for most descriptors especially when using a single operator. Most variants such as LTP, CLBP and CLBC achieved classification accuracy less than 60% in single operator and even less than 50% in some case because of the complex characteristics of the data, such as high resolution and nonrigid deformations. The results show the clear superiority of the proposed *Feat − WCLTP* especially with patterns (P = 8, R = 1), where it achieved a considerable improvement rate of about 3% over the WCLTP accuracy rate. In pattern (P = 16, R = 2) the *Feat − WCLTP* achieved the highest classification accuracy, reaching 94.55%, while *WCLTP* achieved 93.48% and *CLTP* achieved 92.6%. Overall, the *Feat − WCLTP* enhanced the performance of *CLTP* and *WCLTP* in all experiments using the UIUC dataset. Generally, the Feat-WCLTP achieved the highest classification accuracy of 95.23%, while *WCLTP* achieved 94.80% and *CLTP* achieved 94.40%

E. EXPERIMENTAL RESULTS ON THE KYLBERG DATASET

The Kylberg dataset consists of 28 classes, where each class contains 160 images. In this experiment, different training images (N = 16, 40, 64, 80) are randomly selected from each class, while the remaining (160-N) images in each class are used for testing. Figure 11 shows some sample images in the Kylberg dataset. To obtain statistically valid experiment results, each random selection is executed 100 times and the average classification rate is used as the final experimental result. Table 6 shows the classification accuracy of Feat-WCLTP and other LBP variants using the Kylberg dataset.

TABLE 5. Classification rates (%) on the UIUC dataset.

Method	Parameters (R,P) . R =the radius of the circle, P =the number of neighbourhood pixels											
	(R=1,P=8)				(R=2,P=16)				(R=3,P=24)			
	5	10	15	20	5	10	15	20	5	10	15	20
LTP	50.06	58.27	64.64	67.8	61.26	71.33	74.4	78.2	60.91	74.53	78.72	83.4
CLBP_S	40.05	47.53	51.63	55.29	41.8	51.34	56.8	60.6	44.87	54.68	60.63	64.2
CLBC_S	39.85	46.69	51.11	55.61	43.37	53.07	59.17	62.39	47.19	57.46	63.48	66.9
CLTP_S	54.29	61.87	69.92	71.6	64.91	75.07	80.48	83.2	68.8	77.6	83.04	86
WCLTP_S	61.65	71.53	76.01	78.61	69.45	78.28	82.53	85.06	72.91	81.15	84.8	87.01
CLBP_M	42.39	49.98	54.45	57.52	56.07	65.65	69.51	72.05	56.15	65.92	71.05	74.37
CLBC_M	39.04	45.51	49.42	52.12	50.67	59.01	64.42	67.1	51.68	60.62	66.63	69.33
CLTP_M	57.49	64.67	69.6	73.6	70.29	79.33	83.36	85.4	69.94	79.33	82.56	85.2
WCLTP_M	66.19	74	77.97	80.28	70.25	77.97	81.8	83.49	69.43	76.83	80.42	82.85
CLBP_M/C	56.92	65.09	69.81	72.66	68.45	76.83	80.14	82.72	68.08	76.75	80.81	83.27
CLTP_M/C	70.06	76.93	80.48	81.8	77.37	83.6	87.04	89.4	76.8	83.47	87.2	88.6
WCLTP_M/C	69.82	77.33	81.5	83.76	75.42	82.75	86.08	87.76	76.15	83.21	86.58	88.41
CLBP_S_M/C	62.52	71.27	75.48	78.65	68.68	77.57	81.36	83.55	69.43	78.61	82.81	85.33
CLTP_S_M/C	68.8	77.33	80.48	83.6	77.37	84.27	87.84	89.8	77.26	84.67	88.48	90.6
WCLTP_S_M/C	72.87	80.24	83.59	86.06	79.05	85.66	89.07	90.77	79.92	86.61	89.58	91.09
CLBP_S/M	64.7	74.65	79.55	82.58	71.8	80.85	85.31	87.6	72.05	82.63	86.88	89.56
CLBC_S/M	65.28	74.88	78.86	82.4	73.16	82.04	86.31	88.51	75.16	83.92	87.68	89.72
CLTP_S/M	65.03	74.4	79.68	83	77.14	85.6	89.44	91.8	79.31	87.73	90.56	93.2
WCLTP_S/M	74.99	82.32	86.12	88.02	82.51	89.15	91.55	92.87	83.8	89.92	92.27	93.8
CLBP_S/M/C	74.53	82.26	85.85	87.86	78.75	86.33	89.25	91.03	78.05	85.87	89.17	91.07
CLBC_S/M/C	74.57	82.35	85.66	87.83	79.48	86.63	89.66	91.04	79.75	86.45	90.1	91.39
CLTP_S/M/C	74.51	81.73	85.92	86.8	82.63	87.87	90.4	92.6	82.97	88.93	91.52	94.4
WCLTP_S/M/C	77.55	84.72	87.68	89.28	84.21	90.11	92.28	93.48	84.63	90.22	92.72	94.8
Feat-WCLTP_S/M/C	**80.58**	**87.92**	**90.62**	**92.16**	**84.32**	**91.03**	**93.48**	**94.55**	**83.94**	**91.15**	**93.76**	**95.23**

Bold values indicate the best result
* The results for LTP from [21]
* The results for CLBP, CLBC and CLTP from [29]

TABLE 6. Classification rates (%) on the Kylberg dataset.

Method	**Parameters (R,P) . R =the radius of the circle, P =the number of neighbourhood pixels**											
	(R=1,P=8)				**(R=2,P=16)**				**(R=3,P=24)**			
	16	**40**	**64**	**80**	**16**	**40**	**64**	**80**	**16**	**40**	**64**	**80**
CLBP_S	90.58	95.03	96.47	97.03	90.13	95.06	96.76	97.4	93.27	97.1	98.13	98.44
CLTP_S	90.63	94.97	96.36	96.84	95.73	98.35	99.01	99.2	96.86	99.18	99.52	99.6
WCLTP_S	93.11	96.64	97.61	98.01	95.56	98.53	99.14	99.31	95.78	98.71	99.33	99.47
CLBP_M	85.68	91.34	93.38	94.09	91.52	95.23	96.45	96.89	93.11	95.72	96.57	96.99
CLTP_M	93.01	96.82	97.86	98.23	96	98.28	98.87	99.08	97.19	98.99	99.35	99.47
WCLTP_M	94.44	97.04	97.97	98.32	96.49	98.3	98.87	98.99	96.98	98.76	99.2	99.36
CLBP_M/C	94.54	97.46	98.31	98.58	96.4	98.37	98.9	99.14	97.28	98.94	99.35	99.51
CLTP_M/c	95.92	98.03	98.72	98.87	97.58	98.88	99.28	99.4	98.21	99.36	99.62	99.66
WCLTP_M/C	96.19	98.28	98.96	99.22	97.48	99.03	99.49	99.62	98.46	99.41	99.68	99.73
CLBP_S_M/C	96.11	98.35	98.98	99.14	96.43	98.72	99.33	99.45	97.26	99.07	99.46	99.62
CLTP_S_M/C	95.94	98.02	98.62	98.82	97.46	98.98	99.37	99.51	97.92	99.41	99.67	99.75
WCLTP_S_M/C	96.2	98.21	98.87	99.14	97.36	99.12	99.53	99.66	98.05	99.36	99.69	99.7
CLBP_S/M	96.07	98.53	99.08	99.32	97.71	99.3	99.65	99.75	97.96	99.46	99.77	99.82
CLTP_S/M	95.21	97.85	98.6	98.8	97.58	99.31	99.65	99.75	98.11	99.54	99.78	99.8
WCLTP_S/M	96.56	98.65	99.21	99.37	97.88	99.42	99.67	99.76	98.17	99.58	99.72	99.81
CLBP_S/M/C	97.34	99.24	99.6	99.7	98.35	99.55	99.79	99.84	98.62	99.6	99.78	99.83
CLTP_S/M/C	96.61	98.39	98.92	99.11	98.36	99.49	99.71	99.78	98.67	99.65	99.82	99.87
WCLTP_S/M/C	**97.32**	98.97	**99.74**	**99.84**	**98.46**	**99.63**	99.79	**99.86**	**98.79**	99.68	99.84	99.88
Feat-WCLTP_S/M/C	97.27	**99.01**	99.4	99.53	98.39	99.55	**99.82**	99.83	98.71	**99.83**	**99.88**	**99.92**

*Bold values indicate the best result

Table 6 clearly shows that almost all descriptors performed well on the Kylberg dataset. The proposed Feat-WCLTP and WCLTP achieved impressive results in most cases. The best classification result was obtained by $Feat - WCLTP\_S/M/C_{24,3}$ of 99.92%, and 99.88% for $WCLTP\_S/M/C_{24,3}$. with a slight difference of 0.01% for the $CLTP\_S/M/C_{24,3}$. In general, the best result was achieved by $Feat - WCLTP$ with an accuracy of 99.92%, followed by $WCLTP$ (99.88%) and $CLTP$ (99.87%) for pattern size (R = 3, P = 24) when 80 images were used for training.

F. DIMENSIONALITY COMPARISON

The previous experimental results indicate the effectiveness of the proposed descriptors in improving the classification accuracy of the CLTP descriptor. The high dimensionality increases the computational complexity of the descriptor and slows down the classification process. The term 'dimensionality' denotes the number of extracted features, which is the size of the histogram that represents the image features. Figure 12 shows a dimensionality comparison between the proposed descriptors and CLTP when using a multi-scale

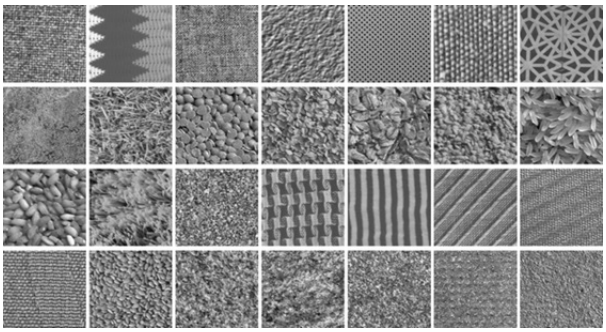

FIGURE 11. Some images from Kylberg dataset.

of R. The histogram size increased sharply when the radius increased. At R = 1 and P = 8, both CLTP and WCLTP have the same size of 400 bins, while the Feat-WCLTP has a size of 160 bins. When the R increased to = 4, the histogram size of the proposed WCLTP exceeded 4500, while the size of Feat-WCLTP was less than 550 bins. Thus, the proposed Feat-WCLTP successfully reduced the dimensionality even when a multi-scale of radii was used, and it achieved higher accuracy classification rates in many cases or maintained the same performance of WCLTP in a few cases. A large number of bins is needed in terms of P = 16 or P = 24. Also, it can be observed that increasing the value of P increased the histogram size considerably. For example, in the pattern (R = 4 and P = 24), the WCLTP histogram size exceeded 38000 bins, while the histogram size for Feat-WCLTP was only around 1500 bins. This significant difference proved

TABLE 7. The number of bins and classification running time using OuTex TC10 dataset.

Pattern size	Dimensionality / Time (seconds)	CLBP	CLTP	WCLTP	Feat-WCLTP
R=1, P=8	No. of bins	200	400	400	160
	Classification Time.	2.14	17.89	16.125	2.1
R=2, P=16	No. of bins	2,312	4,624	4,624	544
	Classification Time.	30.24	72.12	71.35	10.4
R=3, P=24	No. of bins	10,952	21,904	21,904	1,184
	Classification Time.	82.37	172	169	16.8

the efficiency of Feat-WCLTP in reducing the high dimensionality of WCLTP. Increasing the number of bins and size of the descriptor will reflect on its performance, as shown with CLBP and CLTP in the texture datasets. Moreover, this will affect the computation complexity and storage space. To confirm the priority of the Feat-WCLTP, the experiments in the next section compare the classification time cost of the proposed descriptors and of CLTP.

G. CLASSIFICATION TIME COST

The classification time of the proposed descriptors and CLTP is computed using OuTex TC_10 with different pattern sizes. this experiment was performed using MATLAB on a PC with 3.40 GHz Intel®Core^{TM} i7-2600 CPU and 4 GB RAM. Figure 13 shows a classification time comparison between the proposed WCLTP, Feat-WCLTP and CLTP using the OuTex dataset.

Figure 13 shows that the Feat-WCLTP is faster than WCLTP and CLTP in all experiments. When using P = 8, the time cost for both CLTP and WCLTP for texture

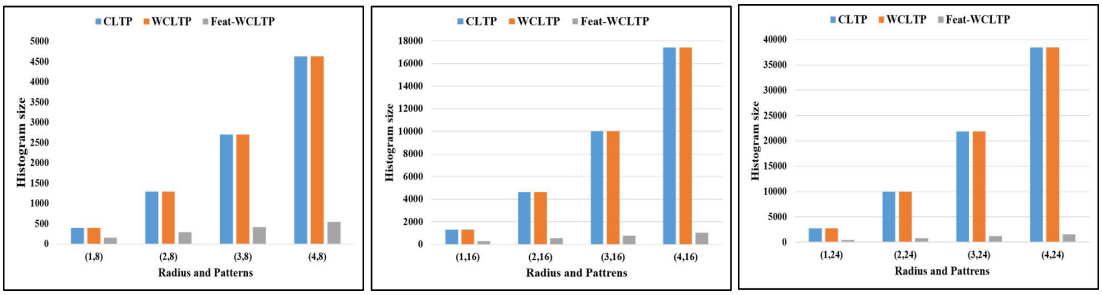

FIGURE 12. Dimensionality comparison of proposed descriptors with CLTP.

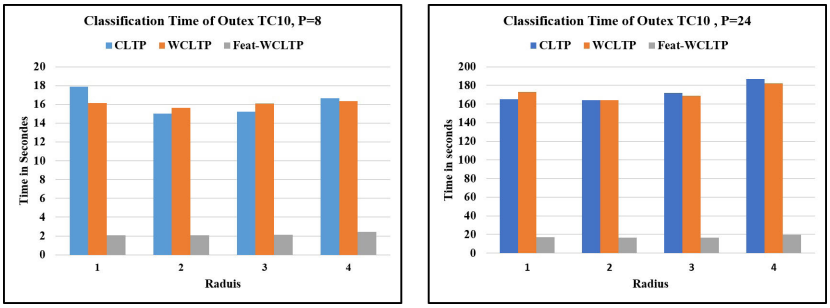

FIGURE 13. Classification time comparison of proposed descriptors and CLTP using OuTex dataset with different radius (i.e. R=1,2,3,4).

TABLE 8. The best classification accuracy on benchmark datasets.

Number	Dataset	Classes	CLBP	CLTP	WCLTP	Feat-WCLTP
1	OuTex	24	99.32%	99.17%	99.35%	**99.66%**
3	CUReT	61	94.74%	96.11%	96.57%	**96.89%**
4	UIUC	25	91.07%	94.40%	94.80%	**95.23%**
5	Kylberg	28	99.83%	99.87%	99.88%	**99.92%**

classification is around four times that of Feat-WCLTP. The minimum classification time consumed by Feat-WCLTP was around 2.1 seconds, while the maximum of around 16.37 seconds was consumed by WCLTP. The classification time for CLTP and WCLTP using P = 24 is about 10 times that for Feat-WCLTP because of the number of extracted features fed to the classifier. The maximum classification time is around 187 seconds for CLTP and around 182 seconds for WCLTP, whereas it is only about 20 seconds for Feat-WCLTP when P = 24 and R = 4.

The following table shows a comparison of the number of bins and classification running time of the proposed descriptors, CLTP and CLBP.

Table 7 shows the superiority of Feat-WCLTP in reducing the dimensionality, which minimises the classification time. The Feat-WCLTP obtained the minimum classification time (2.1 seconds) and the minimum number of bins (160) with pattern (R = 1, P = 8). While CLTP obtained the maximum classification time (172 seconds) and 21,904 bins with the pattern (R = 3, P = 24).

The following table shows the best classification results on all used benchmark datasets. Table 8 shows that Feat-WCLTP performs best in all datasets. Feat-WCLTP achieved the highest classification rate of 99.92% in all datasets, particularly in the Kylberg dataset.

V. CONCLUSION

In this paper, a new descriptor for texture classification, namely, Feat-WCLTP has been proposed. The proposed descriptor could provide high classification performance with lowest histogram size. The main motivation of this paper was to handle the dimensionality problem as well as enhancing the classification accuracy of one of the previous descriptors which is CLTP by introducing a new descriptor (Feat-WCLTP). In the Feat-WCLTP descriptor, the redundant discrete wavelet transform RDWT is integrated with the original CLTP. Then, the mean and variance features are used to describe the magnitude information instead of using P-dimensional features as the normal magnitude components of CLTP. Using these two features helps to reduce the dimensionality of CLTP as well as improve the performance since they provide better complementarity to the sign information. Finally, the centre information also included and used to build the centre operator. The three Feat-WCLTP operators are combined to represent the final histogram. To assess the performance of Feat-WCLTP, a series of experiments on various Texture benchmarks datasets were conducted using k-fold cross-validation method. The results show the ability of Feat-WCLTP to generate high classification rate with lowest histogram size compared to other descriptors. Although Feat-WCLTP descriptor achieved good classification performance using the threshold value that was successfully tested and selected in previous research, this fixed value might not be appropriate in different cases. In the future, this limitation may be addressed using optimisation algorithms to select the best threshold value for each dataset.

REFERENCES

[1] Y. Dong, T. Wang, C. Yang, L. Zheng, B. Song, L. Wang, and M. Jin, "Locally directional and extremal pattern for texture classification," *IEEE Access*, vol. 7, pp. 87931–87942, 2019.

[2] D. O. Tambasco Bruno, M. Z. Do Nascimento, R. P. Ramos, V. R. Batista, L. A. Neves, and A. S. Martins, "LBP operators on curvelet coefficients as an algorithm to describe texture in breast cancer tissues," *Expert Syst. Appl.*, vol. 55, pp. 329–340, Aug. 2016.

[3] T. H. Rassem, B. Ee Khoo, M. F. Mohammed, and N. M. Makbol, "Medical, scene and event image category recognition using completed local ternary patterns (CLTP)," *Malaysian J. Comput. Sci.*, vol. 30, no. 3, pp. 200–218, Nov. 2017.

[4] H. Erfankhah, M. Yazdi, M. Babaie, and H. R. Tizhoosh, "Heterogeneity-aware local binary patterns for retrieval of histopathology images," *IEEE Access*, vol. 7, pp. 18354–18367, 2019.

[5] X. Wang, T. X. Han, and S. Yan, "An HOG-LBP human detector with partial occlusion handling," in *Proc. IEEE 12th Int. Conf. Comput. Vis.*, Sep. 2009, pp. 32–39.

[6] V. Kellokumpu, G. Zhao, and M. Pietikäinen, "Recognition of human actions using texture descriptors," *Mach. Vis. Appl.*, vol. 22, no. 5, pp. 767–780, Sep. 2011.

[7] M. Ruiz, L. E. Mujica, S. Alférez, L. Acho, C. Tutivén, Y. Vidal, J. Rodellar, and F. Pozo, "Wind turbine fault detection and classification by means of image texture analysis," *Mech. Syst. Signal Process.*, vol. 107, pp. 149–167, Jul. 2018.

[8] Y. Liu, G. Liu, C. Liu, and C. Sun, "A novel color-texture descriptor based on local histograms for image segmentation," *IEEE Access*, vol. 7, pp. 160683–160695, 2019.

[9] R. M. Anwer, F. S. Khan, J. Van De Weijer, M. Molinier, and J. Laaksonen, "Binary patterns encoded convolutional neural networks for texture recognition and remote sensing scene classification," *ISPRS J. Photogramm. Remote Sens.*, vol. 138, pp. 74–85, Apr. 2018.

[10] O. Zoidi, N. Nikolaidis, A. Tefas, and I. Pitas, "Stereo object tracking with fusion of texture, color and disparity information," *Signal Process., Image Commun.*, vol. 29, no. 5, pp. 573–589, May 2014.

[11] Y. Liang, Y. Li, K. Zhao, and L. Meng, "Object tracking algorithm based on multi-channel extraction of AHLBP texture features," in *Proc. Int. Conf. Adv. Mech. Syst. (ICAMechS)*, Aug. 2018, pp. 332–336.

[12] T. H. Rassem, N. M. Makbol, and S. Y. Yee, "Face recognition using completed local ternary pattern (CLTP) texture descriptor," *J. Elect. Comput. Eng.*, vol. 7, no. 3, p. 1594, Oct. 2017.

[13] M. A. Abuzneid and A. Mahmood, "Enhanced human face recognition using LBPH descriptor, multi-KNN, and back-propagation neural network," *IEEE Access*, vol. 6, pp. 20641–20651, 2018.

[14] W. Li, H. Pan, P. Li, X. Xie, and Z. Zhang, "A medical image retrieval method based on texture block coding tree," *Signal Process., Image Commun.*, vol. 59, pp. 131–139, Nov. 2017.

[15] P. Liu, J.-M. Guo, K. Chamnongthai, and H. Prasetyo, "Fusion of color histogram and LBP-based features for texture image retrieval and classification," *Inf. Sci.*, vol. 390, pp. 95–111, Jun. 2017.
[16] H. Zhou, R. Wang, and C. Wang, "A novel extended local-binary-pattern operator for texture analysis," *Inf. Sci.*, vol. 178, no. 22, pp. 4314–4325, Nov. 2008.
[17] P. Yang, F. Zhang, and G. Yang, "Fusing DTCWT and LBP based features for rotation, illumination and scale invariant texture classification," *IEEE Access*, vol. 6, pp. 13336–13349, 2018.
[18] L. Liu, J. Chen, P. Fieguth, G. Zhao, R. Chellappa, and M. Pietikäinen, "From BoW to CNN: Two decades of texture representation for texture classification," *Int. J. Comput. Vis.*, vol. 127, no. 1, pp. 74–109, Jan. 2019.
[19] T. Ojala, M. Pietikainen, and T. Maenpaa, "Multiresolution gray-scale and rotation invariant texture classification with local binary patterns," *IEEE Trans. Pattern Anal. Mach. Intell.*, vol. 24, no. 7, pp. 971–987, Jul. 2002.
[20] T. Ojala, M. Pietikäinen, and D. Harwood, "A comparative study of texture measures with classification based on featured distributions," *Pattern Recognit.*, vol. 29, no. 1, pp. 51–59, Jan. 1996.
[21] X. Tan and W. Triggs, "Enhanced local texture feature sets for face recognition under difficult lighting conditions," *IEEE Trans. Image Process.*, vol. 19, no. 6, pp. 1635–1650, Feb. 2010.
[22] T. Ahonen and M. Pietikäinen, "Soft histograms for local binary patterns," in *Proc. Finnish signal Process. Symp. (FINSIG)*, 2007, vol. 5, no. 9, pp. 1–4.
[23] J. Ren, X. Jiang, and J. Yuan, "Noise-resistant local binary pattern with an embedded error-correction mechanism," *IEEE Trans. Image Process.*, vol. 22, no. 10, pp. 4049–4060, Oct. 2013.
[24] A. Fathi and A. R. Naghsh-Nilchi, "Noise tolerant local binary pattern operator for efficient texture analysis," *Pattern Recognit. Lett.*, vol. 33, no. 9, pp. 1093–1100, Jul. 2012.
[25] L. Liu, P. Fieguth, Y. Guo, X. Wang, and M. Pietikäinen, "Local binary features for texture classification: Taxonomy and experimental study," *Pattern Recognit.*, vol. 62, pp. 135–160, Feb. 2017.
[26] Z. Guo, L. Zhang, and D. Zhang, "A Completed modeling of local binary pattern operator for texture classification," *IEEE Trans. Image Process.*, vol. 19, no. 6, pp. 1657–1663, Jun. 2010.
[27] Y. Zhao, D.-S. Huang, and W. Jia, "Completed local binary count for rotation invariant texture classification," *IEEE Trans. Image Process.*, vol. 21, no. 10, pp. 4492–4497, Oct. 2012.
[28] T. H. Rassem and B. E. Khoo, "Completed local ternary pattern for rotation invariant texture classification," *Sci. World J.*, vol. 2014, pp. 1–10, 2014.
[29] Z. Pan, Z. Li, H. Fan, and X. Wu, "Feature based local binary pattern for rotation invariant texture classification," *Expert Syst. Appl.*, vol. 88, pp. 238–248, Dec. 2017.
[30] M. Irani Mehr, M. A. Riahi, and A. Goudarzi, "Innovative RDWT: A new DWT-based method with applications for seismic ground roll attenuation," *J. Geophys. Eng.*, vol. 10, no. 4, Aug. 2013, Art. no. 045004.
[31] J. Fowler, "The redundant discrete wavelet transform and additive noise," *IEEE Signal Process. Lett.*, vol. 12, no. 9, pp. 629–632, Sep. 2005.
[32] L. Liu, Y. Long, P. W. Fieguth, S. Lao, and G. Zhao, "BRINT: Binary rotation invariant and noise tolerant texture classification," *IEEE Trans. Image Process.*, vol. 23, no. 7, pp. 3071–3084, Jul. 2014.
[33] A. Shamaileh, T. H. Rassem, I. A. Ahmed, and K. M. Alalayah, "Wavelet completed local ternary pattern (WCLTP) for texture image classification," *Adv. Sci. Lett.*, vol. 24, no. 10, pp. 7675–7681, Oct. 2018.
[34] K. J. Dana, B. Van Ginneken, S. K. Nayar, and J. J. Koenderink, "Reflectance and texture of real-world surfaces," *ACM Trans. Graph.*, vol. 18, no. 1, pp. 1–34, 1999.
[35] T. Ojala, T. Maenpaa, M. Pietikainen, J. Viertola, J. Kyllonen, and S. Huovinen, "Outex-new framework for empirical evaluation of texture analysis algorithms," in *Proc. Object Recognit. Supported User Interact. Service Robots*, vol. 1, Aug. 2002, pp. 701–706.
[36] S. Lazebnik, C. Schmid, and J. Ponce, "A sparse texture representation using local affine regions," *IEEE Trans. Pattern Anal. Mach. Intell.*, vol. 27, no. 8, pp. 1265–1278, Aug. 2005.
[37] G. Kylberg, *Kylberg Texture Dataset v. 1.0. Centre for Image Analysis*. Uppsala, Sweden: Swedish Univ. of Agricultural Sciences, 2011.

ABEER MOH'D SHAMAILEH received the B.S. degree in computer engineering from Muthah University, Al Karak, Jordan, in 2011, and the M.Sc. degree in computer science from Universiti Mayaysia Pahang (UMP), Kuantan, Malaysia, in 2019. Her research interests include image texture classification and neural networks.

TAHA H. RASSEM (Senior Member, IEEE) received the B.Sc. degree in computer engineering from the University of Technology, Baghdad, Iraq, in 2001, the M.Tech. degree in computer science from the University of Hyderabad, Hyderabad, India, in 2007, and the Ph.D. degree from the School of Electrical and Electronic Engineering (Computer Engineering- Image Processing) from Universiti Sains Malaysia, in 2014. He was an Assistant Lecturer at the Computer Engineering Department, School of Computer Science and Engineering, Hodeidah University, Hodeidah, Yemen, from 2001 to 2005. He is currently a Senior Lecturer in the graphics and multimedia program with the Faculty of Computing, Universiti Malaysia Pahang (UMP). He published many research papers in many ISI and Scopus indexed journal as well as a committee member in many of the international conferences. His research interests are in the area of image classification, object recognition, deep learning, natural language processing, and computer vision. He is a Senior Member of the IAENG and ASR, and a member of the MBOT.

LIEW SIAU CHUIN received the B.IT. degree from the University of Southern Queensland, Australia, the M.Sc. degree in strategic business IT from the University of Portsmouth, U.K., and the Ph.D. degree in computer science from the University of Portsmouth. He is currently a Senior Lecturer at the Faculty of Computing, Universiti Malaysia Pahang, Malaysia. His research interest is in the area of image processing, especially in medical image processing.

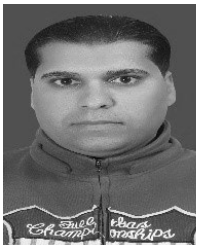

OSAMA NAYEL AL SAYAYDEH received the B.S. degree in computer science from Mutah University, Al Karak, Jordan, in 2007, the M.Sc. degree in computer science from Al al-BAYT University, Al Mafraq, Jordan, in 2011, and the Ph.D. degree in computer science from Universiti Malaysia Pahang (UMP), Kuantan, Malaysia, in 2019. His research interests include pattern classification, neural networks, fuzzy neural networks, and image texture classification.